Modeling and Harmonic Optimization of a Two-Stage Saturable Magnetically Controlled Reactor for an Arc Suppression Coil

Xuxuan Chen, *Member, IEEE*, Baichao Chen, Cuihua Tian, Jiaxin Yuan, *Member, IEEE*, and Yaozhong Liu

***Abstract*—Magnetically controlled reactors (MCRs) are usually used as three-phase shunt reactors. They have low harmonic distortion independent of the third harmonic current because most three-phase MCRs are delta connected. However, as arc suppression coils, MCRs are operated in the single-phase mode, and the harmonics can be much higher than those of three-phase MCRs. In this paper, the structure and the mathematical model of a two-stage saturable MCR (TSMCR) are proposed. There are two stages with different lengths and areas in the iron cores. The stages saturate at different times when the TSMCR outputs reactive current. The current harmonics of the first saturated stage can be compensated for when the second stage begins to saturate, to reduce the total harmonics of the output current. The mathematical model that reveals the distribution characteristics of the current harmonics for the TSMCR is also presented. A study of the mathematical model indicates that there are two key factors that affect the total current harmonics of the TSMCR. One is the parameter k, which represents the area ratio of the second stage to the first stage. The other one is the parameter m, which represents the ratio of the length of the first stage to the total length of the magnetic valve in the iron core. The simulations and experiments show that the maximum current harmonics of the novel MCR can be limited to 3.61% of the rated output current when k and m are chosen according to the theoretical mathematical model.**

***Index Terms*—Arc suppression coil, harmonic analysis, magnetically controlled reactor (MCR), magnetic variable control, saturable reactor (SR).**

I. Introduction

ARC suppression coils are used to reduce the single-phase ground fault current so that nonpermanent faults can be self-extinguished without break operations [1]–[4]. The working principle of arc suppression coils is that the capacitive earth fault current can be compensated for by injecting an inductive current. Usually, these fixed reactors known as Petersen coils are installed at transformer neutrals. However, in order to avoid resonance problems in the distribution network of neutral resonant grounding, the off-tuning degree defined as the ratio of the difference of the fault capacitive current and the inductive current to the capacitive current is usually set to the value of 5%, and this will result in difficulty to self-extinguish the fault arcs [5]. Considering the aforementioned problems, an arc-quenching device with an adjustable reactance, known as a controlled reactor, is attractive in the presence of a fault current that may exceed the admissible limits due to the installation of additional transmission lines or cables.

Conventional adjustable arc suppression coils cannot compensate for the capacitive current efficiently because most of them are controlled manually, and the reactive current that they provide does not fit the fault current smoothly. Research efforts to implement a continuous and low-distortion current of the controlled reactor have been reported in the literature [6]–[13]. Among these approaches are the saturable reactor (SR) and the thyristor-controlled reactor (TCR). The TCR is a reactance that is connected in series with a bidirectional thyristor valve. The reactance of a TCR can be controlled by changing the switching angle to regulate the current through the reactor. The magnetically controlled reactor (MCR) is one type of SR that is based on the working principle of a magnetic magnifier. The reactance of an MCR is changed by controlling the dc current through the control winding, which saturates the iron core [7]. The advantage of the MCR over the TCR is that the MCR can be implemented in ultrahigh-voltage (UHV) power systems and is much more economical and operational. However, the current harmonics of the MCRs are high without filters and limit their applications [8].

To reduce the harmonics of these devices, a passive power filter (PPF), which consists of a fixed capacitor connected in series with an inductor, is typically used [14]. However, PPFs operate at fixed resonance frequencies and therefore have the problem of resonance. To solve the resonance problem, active power filters (APFs) and hybrid APFs (HAPFs) were developed [15]–[19]. The working principle of most of these devices is based on the instantaneous reactive power theory, which is used to accurately extract the harmonic components from the measured current [20]. The control strategies of them are also complicated in order to get high dynamic performance [21]. In addition, the cost of APFs and HAPFs is relatively high, and they are not preferable for UHV power systems.

Manuscript received January 31, 2010; revised March 27, 2011 and September 18, 2011; accepted October 3, 2011. Date of publication October 20, 2011; date of current version February 17, 2012. This work was supported by the National Natural Science Foundation of China under Grant 50807041.

X. Chen was with the College of Electrical Engineering, Wuhan University, Wuhan 430073, China. He is now with the Guangxi Electric Power Research Institute, Nanning 530023, China (e-mail: chenxx82@gmail.com).

B. Chen, C. Tian, and J. Yuan are with the College of Electrical Engineering, Wuhan University, Wuhan 430073, China (e-mail: whgycbc@163.com; tch_gr@163.com; yjx98571@163.com).

Y. Liu was with the College of Electrical Engineering, Wuhan University, Wuhan 430073, China. He is now with the Anhui Electric Power Design Institute, Hefei 230000, China (e-mail: Liuyaozhong@163.com).

Color versions of one or more of the figures in this paper are available online at http://ieeexplore.ieee.org.

Digital Object Identifier 10.1109/TIE.2011.2173090

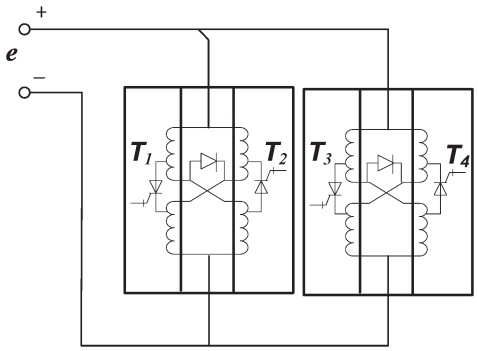

Fig. 1. Traditional compensation method to limit current harmonics in MCRs.

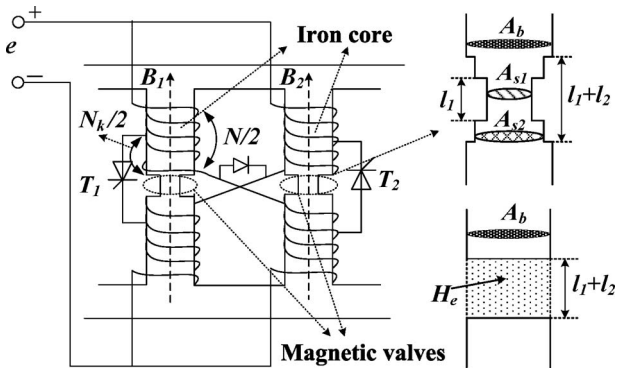

Fig. 2. Model of the TSMCR.

To avoid using any method mentioned above to reduce the harmonics, the current harmonics of MCRs are usually limited by connecting two of them in parallel, as shown in Fig. 1. By controlling the saturation degrees of the iron cores, two MCRs create approximately equal harmonic currents but in opposite directions; thus, the total current harmonics of the MCRs are reduced. However, there are several defects in this combination. The control strategies are complicated if there are too many analog and digital signals; moreover, it also significantly reduces the response time of the MCRs. Additionally, the construction cost is expensive, and the size is inconvenient for indoor installation. One study proposed a new structure of the two-stage saturable MCR (TSMCR) that was implemented for reactive power compensation in an electric railway supply substation [22]. However, the lengths of the two stages in the iron cores are the same, and the area relationship between the two stages is not clear. Thus, the harmonics of the output current do not achieve the desired purpose. The maximum third harmonic component is about 7% of the fundamental current component. The result is almost the same as that of a conventional MCR, which has only one stage in the iron core.

In this paper, the structure and the working principle of the TSMCR are presented. The mathematical model of the TSMCR for harmonic analysis is also given by introducing two parameters: k represents the area ratio of the second stage to the first stage, and m represents the ratio of the length of the first stage to the total length of the magnetic valve in the iron core. The B–H characteristics of the iron cores can be changed by different values of k and m. Different harmonic distribution characteristics of the output current of the TSMCR are achieved when the iron cores become saturated. We proposed an optimization algorithm based on the mathematical model to find a proper set of values of k and m that result in the smallest total harmonic distortion (THD) in the output current of the TSMCR. To verify the validity of the mathematical model, a simulation in MATLAB/Simulink is also presented. Finally, a prototype TSMCR (1000 VA/380 V) has been designed and constructed to test the effectiveness of the harmonic reduction method.

The rest of this paper is organized as follows. In Section II, the structure and the working principle of the TSMCR are described. The parameter m is also introduced in this section. At the end of this section, the B–H characteristic of the iron core is given. In Section III, the mathematical model of the TSMCR for harmonic analysis is given. The parameter k is introduced in the derivation in this section. In Section IV, we successfully determine the proper set of values of k and m using the proposed optimization algorithm. Finally, the simulations and experiments are presented to verify the theoretical analysis.

II. Model of the TSMCR

There is only one stage in each iron core of the conventional MCR. In contrast, there are two stages in the middle of both iron cores to form magnetic valves for the TSMCR. The proposed model is shown in Fig. 2. A_b is the area of the iron core, A_{s1} is the area of the first stage, and A_{s2} is the area of the second stage. The lengths of the first and the second stage are l_1 and l_2, respectively. Control windings are coupled by winding taps on each half of the iron cores, and thyristors are connected between the taps. The turn for each control winding is $N_{k/2}$. High-rated thyristors are not required because the value of $\delta(N_{k/N})$ is usually 5%. Thus, the voltages on the thyristors are very low.

The principle of operation is achieved by changing the magnetic field strength in the iron cores using the dc current through the control winding. The harmonics in the output currents are compensated for automatically when the second stage begins to saturate. A complex controller or control algorithm is not required for the new device to reduce the harmonics in the output current.

The equivalent working circuit of the TSMCR is shown in Fig. 3(a). The commutation circuits when thyristor T_1 or T_2 is conducting are shown in Fig. 3(b) and (c), respectively. The dc control currents i_{k1} and i_{k2} can be regulated by changing the switching angles of the thyristors. As the switching angle of the thyristors increases, the dc control current in the control winding decreases, and the reactance of the reactor increases.

The B–H characteristics of the magnetic valves can be described using the equal magnetic field strength H_e, which assumes that the areas of the first and the second stage are the same as those of the iron cores, as shown in Fig. 2.

When the first stage begins to saturate, we obtain the following equation:

$$\Phi = BA_b = B_0(A_b - A_{s1}) + B_{s1}A_{s1} \tag{1}$$

where B is the magnetic flux density in the iron core, B_0 is the magnetic flux density in the air gap, and B_{s1} is the magnetic flux density in the first stage.

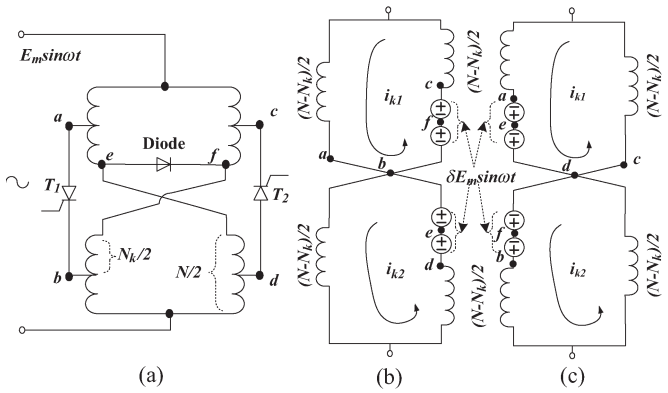

Fig. 3. Equivalent circuit of the TSMCR. (a) Equivalent circuit. (b) T_1 conducted. (c) T_2 conducted.

The magnetic flux density is B_{ts} when the iron core begins to saturate; thus, we have

$$B = \frac{A_b - A_{s1}}{A_b}\mu_0 H_1 + \frac{A_{s1}}{A_b}(\mu_0 H_1 + B_{ts}) \tag{2}$$

where the constant μ_0 is the magnetic permeability in air.

According to Ampere's circuit law

$$H_e(l_1 + l_2) = H_1 l_1. \tag{3}$$

H_e can be rewritten as follows:

$$H_e = \frac{B - \frac{A_{s1}}{A_b}B_{ts}}{\mu_0} \cdot \frac{l_1}{l_1 + l_2}. \tag{4}$$

Similarly, when the second stage begins to saturate, H_e is given as

$$H_e = \frac{B - \frac{A_{s1}}{A_b}B_{ts}\frac{l_1}{l_1+l_2} - \frac{A_{s2}}{A_b}B_{ts}\frac{l_2}{l_1+l_2}}{\mu_0}. \tag{5}$$

Define

$$B_{t1} = \frac{A_{s1}}{A_b}B_{ts} \qquad B_{t2} = \frac{A_{s2}}{A_b}B_{ts} \tag{6}$$

$$m = \frac{l_1}{l_1 + l_2} \qquad 1 - m = \frac{l_2}{l_1 + l_2} \tag{7}$$

where B_{t1} and B_{t2} represent the magnetic flux densities when the first and the second stage begin to saturate, respectively. m represents the ratio of the length of the first stage to the total length.

Then, the B–H characteristics of the magnetic valves, H_e as a function of B, can be written as

$$f(B) = \begin{cases} 0, & |B| < B_{t1} \\ \frac{B - B_{t1}}{\mu_0}m, & B_{t1} \le B < B_{t2} \\ \frac{B - B_{t1}m - B_{t2}(1-m)}{\mu_0}, & B \ge B_{t2} \\ \frac{B + B_{t1}}{\mu_0}m, & -B_{t2} < B \le -B_{t1} \\ \frac{B + B_{t1}m + B_{t2}(1-m)}{\mu_0}, & B \le -B_{t2}. \end{cases} \tag{8}$$

From (8), the B–H characteristics of the magnetic valves are shown in Fig. 4. The gradient of the line between B_{t1} and B_{t2}

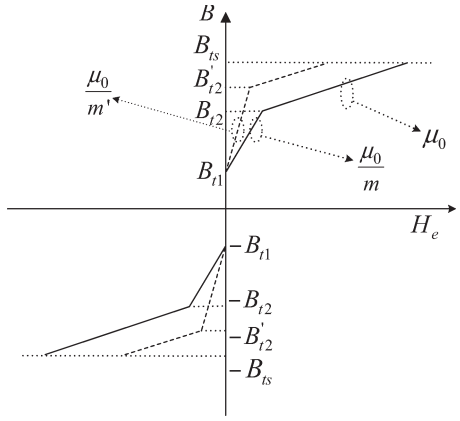

Fig. 4. B–H characteristics of the magnetic valves in the iron cores of the TSMCR.

can be changed by m, and the end of the line can be changed by B_{t2}, which is determined by A_{s1}/A_b. The gradient of the line between B_{t2} and B_{ts} remains unchanged, and the value is a constant μ_0. The dashed line shows the B–H characteristics when the nominal length of the first stage is m' and the area is $A_b B'_{t2}/B_{ts}$.

The magnetic materials used in the iron cores of the TSMCR are the same as those used in modern high-voltage power transformers. However, the operating points of the iron cores in the TSMCR are quite different. The magnetic valves in the iron cores of the TSMCR are deeply saturated, and the magnetic flux density is usually higher than 1.8 T when the TSMCR outputs its rated current. At this scale, hysteresis loops are not significant [23].

III. Harmonics of the TSMCR

The magnetic flux densities B_1 and B_2 in Fig. 2 can be expressed as

$$\begin{cases} B_1(\omega t) = B_d + B_1 \\ B_2(\omega t) = -B_d + B_2 \end{cases} \tag{9}$$

where B_d represents the dc controlled magnetic flux density. The definition of the positive dc control current is shown in Fig. 3.

The analyses of B_1 and B_2 are the same because the structure of the TSMCR is symmetrical. Taking B_1 in the left iron core as an example, as shown in Fig. 5, β_1 and β_2 represent the saturation degrees of the first and the second stage at a power frequency, respectively.

When $B_d = 0$, the stages are not saturated, and $B_1 = B_{t1}\cos(\omega t)$; β_1 and β_2 are given by

$$\begin{cases} \beta_1 = 0, \\ \beta_2 = 0, \end{cases} \qquad B \le B_{t1}. \tag{10}$$

When the first stage begins to saturate and the second stage remains unsaturated, we have

$$\begin{cases} \beta_1 = 2\cos^{-1}\frac{B_{t1} - B_d}{B_{t1}}, \\ \beta_2 = 0, \end{cases} \qquad B_{t1} < B \le B_{t2}. \tag{11}$$

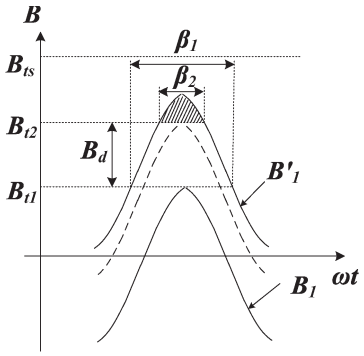

Fig. 5. Relationship between β_1 and β_2.

When the magnetic valves are both saturated, we have

$$\begin{cases} \beta_1 = 2\cos^{-1}\frac{B_{t1}-B_d}{B_{t1}}, \\ \beta_2 = 2\cos^{-1}\frac{B_{t2}-B_d}{B_{t1}}, \end{cases} \qquad B_{t2} \le B \le B_{ts}. \tag{12}$$

From (12), the relationship between β_1 and β_2 can be written as

$$\beta_2 = 2\cos^{-1}\left(\frac{B_{t2}}{B_{t1}} - 1 + \cos\frac{\beta_1}{2}\right). \tag{13}$$

Define $k = B_{t2}/B_{t1}$; from (6), k can be given as

$$k = \frac{B_{t2}}{B_{t1}} = \frac{A_{s2}/A_b}{A_{s1}/A_b} = \frac{A_{s2}}{A_{s1}}. \tag{14}$$

From (13) and (14), the value of β_1 when the second stage begins to saturate, i.e., $\beta_2 = 0$, can be expressed as

$$\beta_{\text{sat}} = 2\cos^{-1}(2-k). \tag{15}$$

Considering that the iron cores cannot be saturated during the regulation, the maximum β_1 is

$$\beta_{\max} = 2\cos^{-1}\left(2 - \frac{A_b}{A_{s1}}\right). \tag{16}$$

From the above and the literature [22], the current harmonic model of the TSMCR can be described as (17), shown at the bottom of the page, where i_1^* represents the nominal fundamental current and i_{2n+1}^* $(n = 1, 2, 3, \ldots)$ represents the nominal current harmonics.

The relationship between β_1 and β_2 in (17) can be expressed as

$$\begin{cases} \beta_2 = 0, & \beta_1 \in [0, \beta_{\text{sat}}] \\ \beta_2 = 2\cos^{-1}\left(k - 1 + \cos\frac{\beta_1}{2}\right), & \beta_1 \in (\beta_{\text{sat}}, \beta_{\max}]. \end{cases} \tag{18}$$

The minimum current THD value of the TSMCR in relation to the rated current can be given as

$$\begin{cases} i_{\text{thd}} = \sqrt{\sum_{j=1}^{\infty}\left(i_{2j+1}^*\right)^2} \Big/ i_{\text{rated}}^* \\ i_{\max} = \max\limits_{\beta_1 \in [0, \beta_{\max}]}(i_{\text{thd}}) \\ i_{\text{opt}} = \min\limits_{k \in (1,3), m \in (0,1)}(i_{\max}) \end{cases} \tag{19}$$

where $i_{\text{rated}}^* = \max(i_1^*)$.

In (19), i_{rated}^* varies for each set value of k and m when β_1 ranges from zero to $\beta_{\max}$. The constraints of k have physical meanings. Because the iron cores cannot be saturated during the regulation, i.e., $\beta_{\max}$ is restricted by A_b/A_{s1}, its value cannot exceed 2π. From (16), the maximum ratio between the iron core and the first stage can be obtained, and its value is three. The area of the second stage is larger than that of the first stage but less than that of the iron core; thus, k is limited between one and three. The physical meaning of m is clear when the sum of $l_1/(l_1+l_2)$ and $l_2/(l_1+l_2)$ is one. If any of the values is zero, only one stage is assumed to exist. For each set value of k and m, there is a maximum value $i_{\max}$ of the total harmonics i_{thd} during the regulation of β_1 from zero to $\beta_{\max}$. The minimum value i_{opt} of $i_{\max}$ can be obtained when k and m are different. i_{opt} will also has different values if $\beta_{\max}$ is considered.

IV. Analysis, Simulation, and Experimental Results

A. Analysis of the Mathematical Model

The current harmonics of the TSMCR are determined by the parameters k and m from (17)–(19). The values of $i_{\max}$ are different when k and m change. Thus, we can obtain the optimal values of the area ratio k and the ratio of the length m that result in a minimum value of $i_{\max}$. The flowchart of the optimization algorithm to find these parameters is shown in Fig. 6. There are external and internal iterations in this algorithm. The external iterations determine the values of k. For each value of k, the internal iterations calculate the minimum value of $i_{\max}$ by changing the value of m. The value i_{opt} is the minimum value of all recorded results when the values of k are different in the external iteration. The accepted step values of k and m are both 0.01. More precise results can be obtained by reducing the step size. The calculation results show that the minimum value i_{opt} occurs when $k = 1.9$ and $m = 0.37$. The values of $i_{\max}$ obtained as a function of K and m are shown in Fig. 7 based on the assumption that $A_b/A_{s1} = 3$ $(\beta_{\max} = 2\pi)$. The area ratio k is replaced by K $(K = k-1)$ in Fig. 7.

The harmonic distribution in the output current of the TSMCR when $k = 1.9$ $(K = 0.9)$ and $m = 0.37$ is shown in Fig. 8. Two wave crests can be obtained in the total harmonic

$$\begin{cases} i_1^* = \frac{1}{2\pi}\left[(\beta_1 - \sin\beta_1)m + (\beta_2 - \sin\beta_2)(1-m)\right] \\ i_{2n+1}^* = \frac{m}{(2n+1)\pi}\left\{\frac{\sin(n\beta_1)}{2n} - \frac{\sin[(n+1)\beta_1]}{2(n+1)}\right\} + \frac{1-m}{(2n+1)\pi}\left\{\frac{\sin(n\beta_2)}{2n} - \frac{\sin[(n+1)\beta_2]}{2(n+1)}\right\} \end{cases} \tag{17}$$

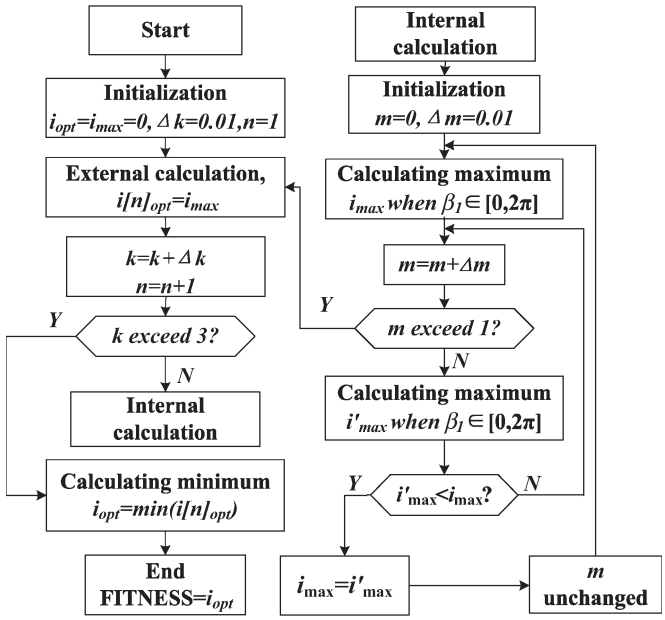

Fig. 6. Flowchart of the optimization algorithm of the TSMCR.

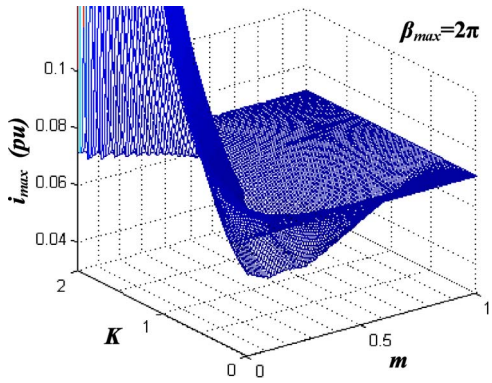

Fig. 7. Relationships among the minimum current THD, the area ratio, and the length ratio.

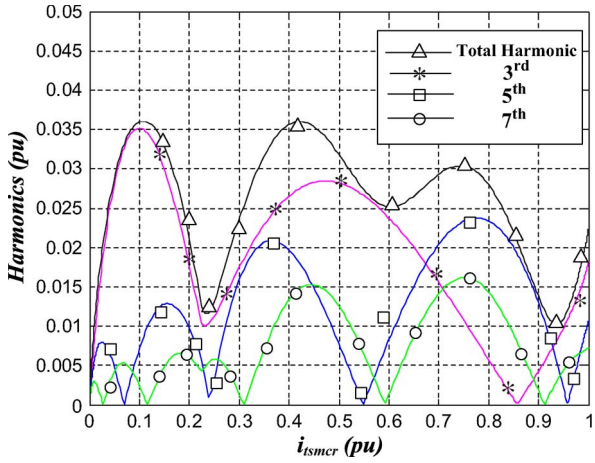

Fig. 8. Harmonic analysis (third, fifth, and seventh) of the current of the TSMCR.

curve, and both of their values are 3.61% of i^*_{rated}. More values of i_{opt} are listed in Table I when the values of A_b/A_{s1} are different.

TABLE I
VALUES OF i_{opt} WHEN $\beta_{\max}$ RANGES FROM π TO 2π

A_b/A_{s1}	β_{max}	$i_{opt}(\%)$
2	3.1416 (π)	11.34
2.2	3.5443	8.08
2.4	3.9646	6.17
2.6	4.4286	4.96
2.8	4.9962	4.16
2.9	5.3811	3.86
3.0	6.2832 (2π)	3.61

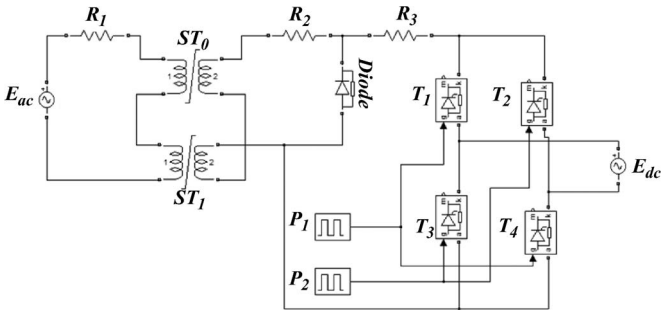

Fig. 9. Simulation model of the TSMCR (1000 VA/380 V).

TABLE II
SIMULATION PARAMETER CONFIGURATION IN MATLAB/SIMULINK

Component	Parameter	Value
E_{ac}	Peak amplitude	537.32 V
E_{dc}	Peak amplitude	29.47 V
R_1, R_2	Resistance	5.15 Ω
R_3	Resistance	0.565 Ω
ST_0, ST_1	Nominal power	500 VA
MCR	Saturation characteristic	[0, 0; 0, 1; 1, 2]
TSMCR	Saturation characteristic	[0, 0; 0, 1; 0.33, 1.9; 1.33, 2.9]

B. Simulation Based on MATLAB/Simulink

A simulation model in MATLAB/Simulink for the TSMCR is shown in Fig. 9. The model is based on the equivalent circuit shown in Fig. 3. The device is modeled by two saturable transformers. In the model, the high-voltage windings are connected with different polarities, and the low-voltage windings are connected with the same polarity. The dc current controller is composed of a single-phase full-bridge controlled rectifier; E_{DC} is about 5% of E_{ac}, which is set by the tap ratio $(N_{k/N})$ of the control winding. The current harmonics of the ac side can be reduced, which is tested and verified by configuring the saturation characteristics of the saturable transformers.

The main simulation parameters are listed in Table II. In this table, the saturation characteristics of both the conventional MCR and the TSMCR are presented.

The output current of the MCRs through the resistor R_1 can be changed smoothly by regulating the switching angles of P_1 and P_2. The waveforms of the output current of both the conventional MCR and the TSMCR are shown in Fig. 10. Based on Fig. 10, we can find that the TSMCR greatly reduces the maximum current harmonics by nearly half compared to those of the conventional MCR. The highest total harmonic

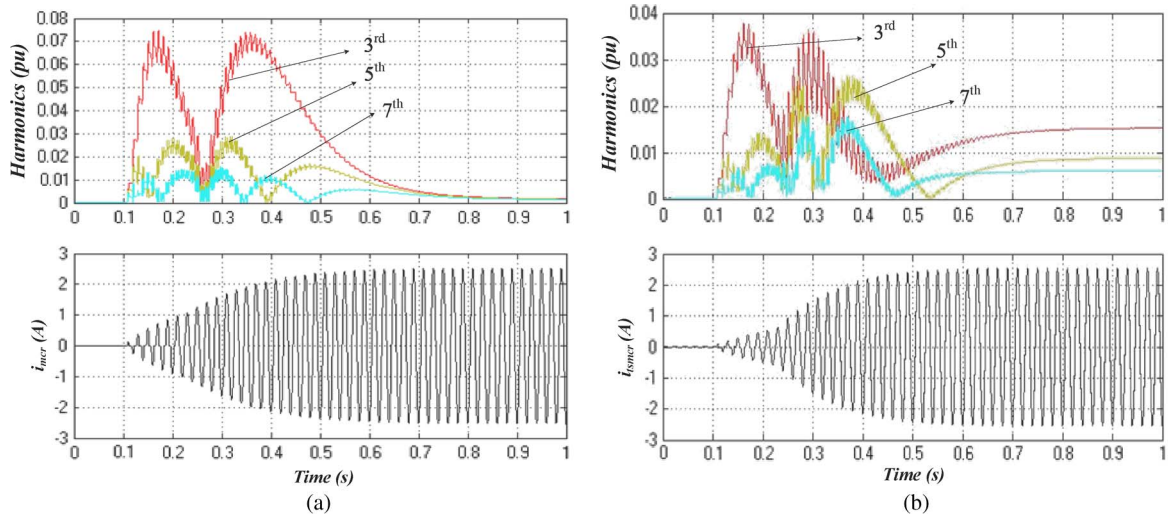

Fig. 10. Current harmonic analyses of the third, fifth, and seventh harmonics in MATLAB when the output current is regulated from zero to rated.

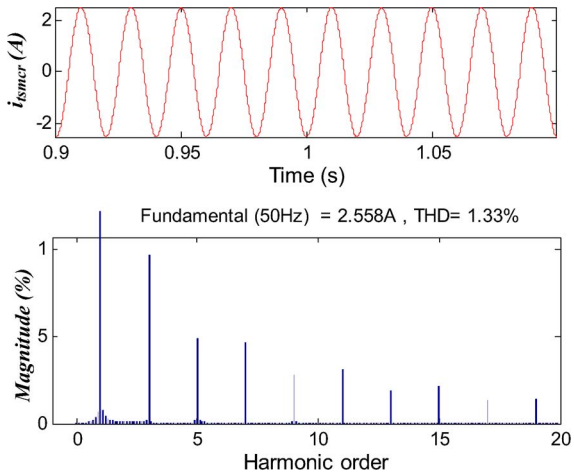

Fig. 11. Fast Fourier transform analysis of the theoretical rated output current of the TSMCR at steady state.

$i_{\max}$ values of the TSMCR and the MCR are 3.6% and 7%, respectively. The simulation results of the TSMCR shown in Fig. 10(b) are the same as the harmonic analysis results shown in Fig. 8. The current harmonic analysis when the TSMCR outputs its rated current in the steady state is also shown in Fig. 11. The current magnitude and THD of i_{tsmcr} are 2.558 A and 1.33%, respectively. The simulation shows that the structure of the TSMCR effectively reduces the current harmonics of conventional MCRs.

The magnetic fluxes of the iron cores are shown in Fig. 12. Curve B_1 begins to increase and B_2 begins to decrease at the same time ($t = 0.1$ s), and both stop changing when $t = 0.9$ s. This result further explains the working principle of the TSMCR: The ac magnetic flux changes smoothly by regulating the switching angle of the thyristors, and a continuous output current i_{tsmcr} can be obtained.

C. Experimental Results

A prototype of the TSMCR (1000 VA/380 V) has been designed and constructed, as shown in Fig. 13.

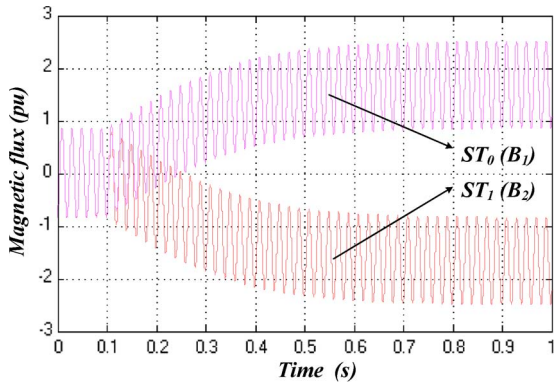

Fig. 12. Magnetic fluxes (B_1 and B_2) in the iron cores of the TSMCR during the regulation when β_1 changes from 0 to 2π.

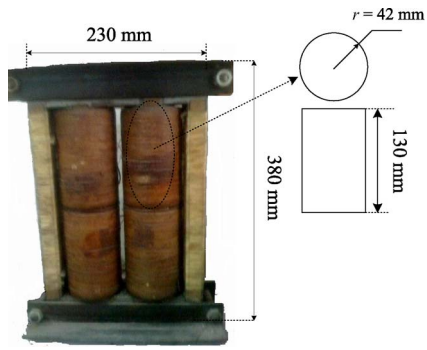

Fig. 13. Prototype of the TSMCR.

The experimental results are shown in Fig. 14. As shown in Fig. 14, the TSMCR greatly reduces the maximum current harmonics i_{thd} (from 7% to 3.6%) during the regulation. We find that the experimental results of the TSMCR are almost the same as the theoretical results shown in Fig. 8. i_{thd} was measured based on several different values of β_1, which were calculated in (9)–(12). The rated output current of the TSMCR is not sinusoidal like the traditional output, but it is still as low as about 2.2%, which can be ignored without the need for a harmonic filter.

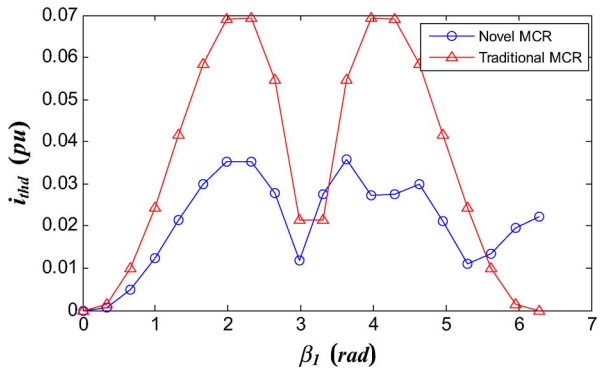

Fig. 14. Current harmonic comparison between the MCR and the prototype TSMCR.

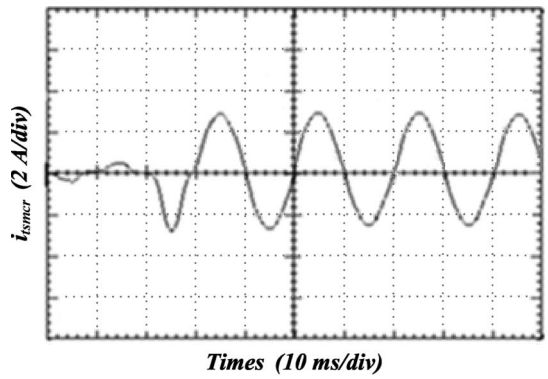

Fig. 15. Transient process of the output current of the TSMCR.

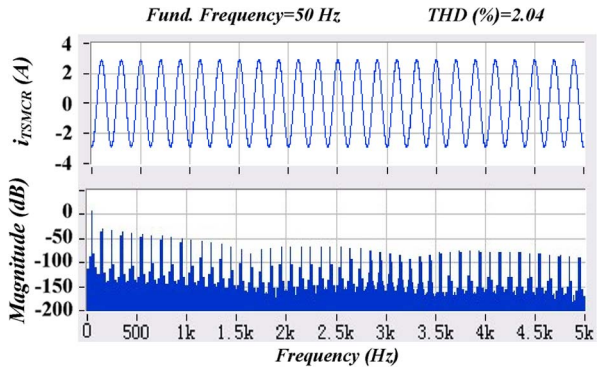

Fig. 16. Distortion of the experimental rated output current of the TSMCR.

The rated output current waveform and its distortion analysis are shown in Figs. 15 and 16, respectively. The curve in Fig. 15 is obtained at the transition when the output current changes from zero to rated using a unique control method. The control method can greatly reduce the transient process of the TSMCR. The current is sinusoidal after $t = 30$ ms. The peak value is 2.89 A, and the THD is 2.04% in Fig. 16. The experimental results are very close to those from simulations.

V. Conclusion

This paper has proposed a method to reduce the harmonics of the MCR that introduces additional stages in the magnetic valves. The theoretical research suggests that there were mainly two parameters that affect the harmonic current.

1) Parameter k ranges from one to three and represents the area ratio of the second stage to the first stage.
2) Parameter m ranges from zero to one and represents the ratio of the length of the first stage to the total length.

Based on the two parameters, the mathematical model for harmonic analysis of the TSMCR has been presented. An optimization algorithm has also been introduced to search for the optimal value of the two parameters k and m, which can be used to reduce the output harmonics of the TSMCR. The results from simulations and experiments show that the reduced harmonic current mainly consists of the third and fifth harmonics after the compensation. The maximum total harmonics can be limited to 3.61% relative to the rated output current of the TSMCR during the regulation without any additional harmonic filter device.

References

[1] B. Gustavsen and J. A. Walseth, "A case of abnormal overvoltages in a Peterson grounded 132-kV system caused by broken conductor," *IEEE Trans. Power Del.*, vol. 18, no. 1, pp. 195–200, Jan. 2003.
[2] J. Tian, Q. Chen, L. Cheng, and Y. Zhang, "Arc-suppression coil based on transformer with controlled load," *IET Elect. Power Appl.*, vol. 5, no. 8, pp. 644–653, Sep. 2010.
[3] R. Burgess and A. Ahfock, "Minimising the risk of cross-country faults in systems using arc suppression coils," *IET Gener., Transm. Distrib.*, vol. 5, no. 7, pp. 703–711, Jul. 2011.
[4] K. J. Sagastabeitia, I. Zamora, A. J. Mazon, Z. Aginako, and G. Buigues, "Phase asymmetry: A new parameter for detecting single-phase earth faults in compensated MV networks," *IEEE Trans. Power Del.*, vol. 26, no. 4, pp. 2251–2258, Oct. 2011.
[5] X. Zeng, Y. Xu, and Y. Wang, "Some novel techniques for insulation parameters measurement and Petersen-coil control in distribution systems," *IEEE Trans. Ind. Electron.*, vol. 57, no. 4, pp. 1445–1451, Apr. 2010.
[6] T. Wass, S. Hornfeldt, and S. Valdemarsson, "Magnetic circuit for a controllable reactor," *IEEE Trans. Magn.*, vol. 42, no. 9, pp. 2196–2200, Sep. 2006.
[7] M. Tian, Q. Li, and Q. Li, "A controllable reactor of transformer type," *IEEE Trans. Power Del.*, vol. 19, no. 4, pp. 1718–1726, Oct. 2004.
[8] R. R. Karymov and M. Ebadian, "Comparison of magnetically controlled reactor (MCR) and thyristor controlled reactor (TCR) from harmonics point of view," *Int. J. Elect. Power Energy Syst.*, vol. 29, no. 3, pp. 191–198, Mar. 2007.
[9] L. Bohmann and R. Lasseter, "Stability and harmonics in thyristor controlled reactors," *IEEE Trans. Power Del.*, vol. 5, no. 2, pp. 1175–1181, Apr. 1990.
[10] A. Garcia-Cerrada, P. Garcia-Gonzalez, R. Collantes, T. Gomez, and J. Anzola, "Comparison of thyristor-controlled reactors and voltage-source inverters for compensation of flicker caused by arc furnaces," *IEEE Trans. Power Del.*, vol. 15, no. 4, pp. 1225–1231, Oct. 2000.
[11] A. Barili, A. Brambilla, G. Cottafava, and E. Dallago, "A simulation model for the saturable reactor," *IEEE Trans. Ind. Electron.*, vol. 35, no. 2, pp. 301–306, May 1988.
[12] N. Ning, X. Li, J. Fan, W. Ng, Y. Xu, X. Qian, and H. Seet, "A tunable magnetic inductor," *IEEE Trans. Magn.*, vol. 42, no. 5, pp. 1585–1590, May 2006.
[13] A. Adly, "Controlling linearity and permeability of iron core inductors using field orientation techniques," *IEEE Trans. Magn.*, vol. 37, no. 4, pp. 2891–2893, Jul. 2001.
[14] L. Zanotto, R. Piovan, V. Toigo, E. Gaio, P. Bordignon, T. Consani, and M. Fracchia, "Filter design for harmonic reduction in high-voltage booster for railway applications," *IEEE Trans. Power Del.*, vol. 20, no. 1, pp. 258–263, Jan. 2005.
[15] S. Ostroznik, P. Bajec, and P. Zajec, "A study of a hybrid filter," *IEEE Trans. Ind. Electron.*, vol. 57, no. 3, pp. 935–942, Mar. 2010.
[16] A. Luo, Z. Shuai, W. Zhu, and Z. Shen, "Combined system for harmonic suppression and reactive power compensation," *IEEE Trans. Ind. Electron.*, vol. 56, no. 2, pp. 418–428, Feb. 2009.

[17] Z. Shu, Y. Guo, and J. Lian, "Steady-state and dynamic study of active power filter with efficient FPGA-based control algorithm," *IEEE Trans. Ind. Electron.*, vol. 55, no. 4, pp. 1527–1536, Apr. 2008.
[18] L. Asiminoaei, E. Aeloiza, P. Enjeti, and F. Blaabjerg, "Shunt active power filter topology based on parallel interleaved inverters," *IEEE Trans. Ind. Electron.*, vol. 55, no. 3, pp. 1175–1189, Mar. 2008.
[19] S. Kim and P. Enjeti, "A new hybrid active power filter (APF) topology," *IEEE Trans. Power Electron.*, vol. 17, no. 1, pp. 48–54, Jan. 2002.
[20] R. S. Herrera and P. Salmern, "Instantaneous reactive power theory: A reference in the nonlinear loads compensation," *IEEE Trans. Ind. Electron.*, vol. 56, no. 6, pp. 2015–2022, Jun. 2009.
[21] A. Bhattacharya and C. Chakraborty, "A shunt active power filter with enhanced performance using ANN-based predictive and adaptive controllers," *IEEE Trans. Ind. Electron.*, vol. 58, no. 2, pp. 421–428, Feb. 2011.
[22] B. Chen and J. Kokernak, "Thyristor controlled two-stage magnetic-valve reactor for dynamic var-compensation in electric railway power supply systems," in *Proc. Appl. Power Electron. Conf. Expo.*, New Orleans, LA, Feb. 2000, vol. 2, pp. 1066–1072.
[23] J. Marti and A. Soudack, "Ferroresonance in power systems: Fundamental solutions," *Proc. Inst. Elect. Eng. C—Gener., Transm. Distrib.*, vol. 138, no. 4, pp. 321–329, Jul. 1991.

Xuxuan Chen (S'09–M'11) received the B.Sc. and Ph.D. degrees from the College of Electrical Engineering, Wuhan University, Wuhan, China, in 2005 and 2011, respectively.

Since 2011, he has been an Engineer with the Guangxi Electric Power Research Institute, Nanning, China. His research interests include power quality issues and electric machine modeling and optimization.

Baichao Chen received the B.Sc. degree in electrical engineering from the Huazhong University of Science and Technology, Wuhan, China, in 1982 and the M.Sc. and Ph.D. degrees from the College of Electrical Engineering, Wuhan University, Wuhan, in 1986 and 1993, respectively.

From 1998 to 1999, he was a Visiting Researcher with the Department of Electrical, Computer, and Systems Engineering, Rensselaer Polytechnic Institute, Troy, NY. He is currently a Professor of electrical engineering with the College of Electrical Engineering, Wuhan University. His main research interests include high-voltage engineering, power quality, and power electronic applications in high-voltage engineering.

Cuihua Tian received the B.Sc., M.Sc., and Ph.D. degrees from the College of Electrical Engineering, Wuhan University, Wuhan, China, in 1992, 1997, and 2005, respectively.

She is currently an Associate Professor of electrical engineering with the College of Electrical Engineering, Wuhan University. Her main research interests include high-voltage engineering, power quality, and microcomputer-based control systems.

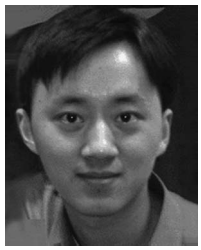

Jiaxin Yuan (M'08) received the B.Sc. and Ph.D. degrees from the College of Electrical Engineering, Wuhan University, Wuhan, China, in 2002 and 2007, respectively.

He is currently an Associate Professor of electrical engineering with Wuhan University. The focus of his research is on power electronic system control, power quality issues, and application and control of inverters.

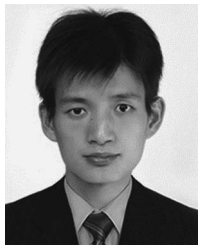

Yaozhong Liu received the B.Sc. and M.Sc. degrees from the College of Electrical Engineering, Wuhan University, Wuhan, China, in 2009 and 2011, respectively.

Since 2011, he has been an Engineer with the Anhui Electric Power Design Institute, Hefei, China. His research interests include overvoltage suppression in power systems, and fault current limiters.